Chapter 2
Zero-Shear Viscosities of Polysaccharide Solutions

Takahiro Sato

Abstract Solution viscosities are strongly dependent on the molecular weight, the concentration, and the chain conformation of polymers added. We have formulated the intrinsic viscosity $[\eta]$ at infinite dilution and the zero-shear viscosity η at finite concentrations using the molecular theory based on the wormlike chain and fuzzy cylinder models. In the theory, the solution viscosity at finite concentrations is affected by both hydrodynamic and entanglement interactions. The formulated viscosity equations quantitatively predict $[\eta]$ and η as functions of the wormlike chain parameters and the strength of the hydrodynamic interaction and demonstrated that the relative importance of the hydrodynamic and entanglement interactions in the solution viscosity depends on the chain stiffness. We have compared the formulated viscosity equations with experimental results for solutions of three polysaccharides and two synthetic polymers covering a wide range of the chain stiffness.

Keywords Intrinsic viscosity • Zero-shear viscosity • Hydrodynamic interaction • Entanglement interaction • Wormlike chain model • Fuzzy cylinder model

2.1 Introduction

Various polysaccharides are contained in foods and drinks and provide unique rheological properties. In many cases, foods and drinks need suitable viscosity to taste comfortably, and polysaccharides are utilized as rheology control reagents for foods and drinks. The addition of polysaccharides remarkably changes viscosities of foods and drinks, and it is well known that the viscosities are strongly dependent on the molecular weight, the concentration, and the chain conformation of polysaccharides added [1].

To understand the viscosity behavior of polysaccharide solutions, the present chapter deals with the molecular theory on the solution viscosity of linear-chain

T. Sato (✉)

Department of Macromolecular Science, Osaka University, 1-1 Machikaneyama-cho, Toyonaka, Osaka 560-0043, Japan

e-mail: tsato@chem.sci.osaka-u.ac.jp

polymers. The polymer conformation ranges from the rigid rod to flexible random coil, and the solution concentration covers from the dilute limit to the concentrated regime just below the phase boundary concentration where the liquid crystal phase appears.

Linear-chain polymers are usually viewed as the wormlike chain model [2] and characterized by the persistence length (or the stiffness parameter) q, the contour length h per monomer unit, and the thickness (or the diameter) b of the wormlike chain, as well as the monomer unit molar mass M_0 and the molecular weight M. The intrinsic viscosity $[\eta]$ characterizing the viscosity of infinitely dilute polymer solution is calculated in terms of these wormlike chain parameters. With increasing the polymer concentration, the intermolecular interaction contributes to the solution viscosity. We can divide the intermolecular interaction into the hydrodynamic interaction and the entanglement interaction. The latter interaction can be treated by the fuzzy cylinder model [3], which is explained below. The Huggins coefficient k' consists of the two interaction terms. The relative importance of the two terms depends on the persistence length q and the contour length $L = hM/M_0$. Finally, the zero-shear viscosity η over a wide concentration range is quantitatively predicted by a viscosity equation derived by a molecular theory.

The present chapter consists of seven sections. After briefly mentioning the solution viscosity behavior of a polysaccharide as a typical example (Sect. 3.2), we present an introduction of viscometry (Sect. 2.3) and definition of the viscosity coefficient (Sect. 2.4) as a basic background to explain the molecular theory. Sections 2.5 and 2.6 deal with the molecular theory for polymer solution viscosity at infinite dilution and at finite concentrations, respectively. In Sect. 2.7, we compare the molecular theory explained with viscosity data for five polymer solution systems of which chain stiffness is largely different and discuss how the concentration, molecular weight, and chain stiffness affect the polymer solution viscosity. Section 2.8 summarizes the results and conclusions explained in this chapter.

2.2 Polysaccharides Used as the Viscosity Enhancement Reagent

Polysaccharides are biopolymers abundant in nature, produced by plants, animals, fungus, algae, and microorganisms [4]. Human beings have used the natural polymers for long years, even before chemists did not verify the existence of polymers. Polysaccharides produced by industrial fermentation, say xanthan (xanthan gum), scleroglucan, and succinoglycan, are utilized as viscosity enhancement reagents adding to foods, cosmetics, paints, cements, and so on. Viscosities of aqueous solutions of xanthan and scleroglucan are stable against changes of temperature, added salt, and pH, while the solution viscosity of succinoglycan is known to collapse at a melting temperature, where this polysaccharide undergoes a structural
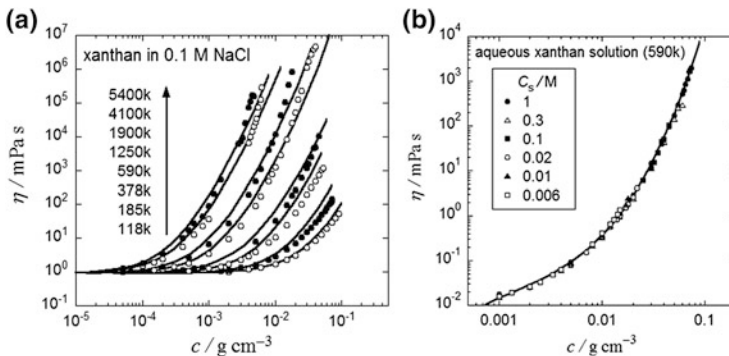
Fig. 2.1 Polymer concentration dependences of the zero-shear viscosity of xanthan in aqueous NaCl solutions; (**a**) data for different molecular weight samples; (**b**) data at different NaCl concentrations [3].

order-disorder transition. The above three polysaccharides are all multistranded helical polymers, and their solution viscosities strongly change by the denaturation of their native helical conformations.

Figure 2.1a shows concentration dependences for 0.1 M aqueous NaCl solutions of xanthan double helices of different molecular weights. In the figure, 5400 k ($=5.4 \times 10^6$) indicates the weight-average molecular weight of the original xanthan sample, and lower molecular weight samples were prepared by sonication of the original sample. For the original xanthan sample, the addition to the aqueous salt solution only by 0.5 wt.% enhances the solution viscosity 10^6 times as high as that of the solvent, but the strong concentration dependence remarkably diminishes with decreasing the molecular weight of the xanthan sample. As mentioned above, the aqueous xanthan solution viscosity is stable by adding salt, in spite of the fact that xanthan is a polyelectrolyte, which is demonstrated in Fig. 2.1b. This is a sharp contrast with the viscosity collapse of aqueous solutions of normal polyelectrolytes by addition of salt. This contrast comes from the stiff double-helical conformation of xanthan.

Because of the strong concentration and molecular weight dependences such as shown in Fig. 2.1a, we can control the viscosity of liquids by adding a small amount of viscosity enhancement reagents. To give a suitable viscosity to liquid products, we have to properly select the kind of viscosity enhancement reagent, as well as its molecular weight and concentration. In what follows, we present a viscosity equation, which gives us a guideline for the selection. Before explaining the viscosity equation, we will review basic knowledge of rheology and molecular theory of polymer solution viscosity.

2.3 Viscometry Using Various Types of Flow

2.3.1 Various Types of Viscometers

There are various types of viscometers, of which principles are illustrated in Fig. 2.2. To determine the viscosity coefficient η, one measures the flow time t for the capillary viscometer (Panel a), falling time t of the ball for falling ball viscometer (Panel b), and the torsional angle Θ of the wire for the coaxial cylinder and corn-and-plate viscometers (Panels c and d). The basic equations to determine η are given by

$$\eta = \begin{cases} \frac{\pi a^4 P}{8lQ} = \frac{\pi a^4 P}{8lV_t}t & \text{(Panel a)} \\ \frac{mg}{6\pi a \upsilon} = \frac{mg}{6\pi aL}t & \text{(Panel b)} \\ \frac{k}{4\pi l\Omega}\left(\frac{1}{r_1^2} - \frac{1}{r_2^2}\right)\Theta & \text{(Panel c)} \\ \frac{3k}{2\pi R^3}\frac{\phi}{\Omega}\Theta & \text{(Panel d)} \end{cases} \tag{2.1}$$
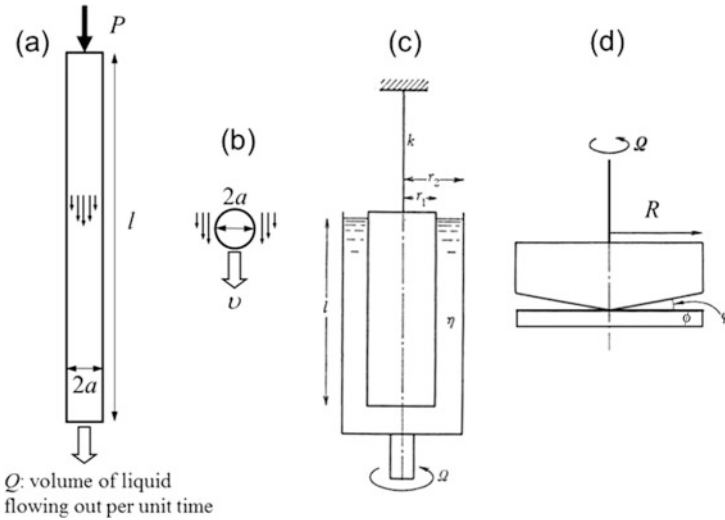

Q: volume of liquid
flowing out per unit time

Fig. 2.2 Schematic diagrams of four types of viscometers: (**a**) the capillary viscometer, where l and a are the length and inner radius of the capillary, P is the pressure difference between the inlet and outlet of the capillary, and Q is the volume of the sample liquid flowing out per unit time ($V_t = Qt$ is the volume of the liquid flowing during time t); (**b**) the falling ball viscometer, where a and υ are the radius and the falling velocity of the ball in the sample liquid ($L = \upsilon t$ is the distance for the ball to fall during time t); (**c**) the coaxial cylinder viscometer, where l and r_1 are the length and radius of the inner cylinder and r_2 and Ω are the radius and angular velocity of the outer cylinder; (**d**) the corn-and-plate viscometer, where R and Ω are the radius and angular velocity of the corn and ϕ is the gap angle between the corn and plate

where m is the mass of the ball, g is the gravitational acceleration, k is the torsional elastic constant of the wire suspending the inner cylinder (Panel c) or the corn (Panel d), and other parameters appearing the equations are explained in the caption of Fig. 2.2. In Fig. 2.1, the data of η lower and higher than 1 mPa·s were obtained by a capillary viscometer in Panel a and by a ball viscometer in Panel b, respectively.

The rate of each flow is characterized by the shear rate $\dot{\gamma}$ of which definition will be given in the next subsection. While the shear rate of the flow in Panel d is uniform within the sample liquid, $\dot{\gamma}$ of the flows in Panels a–c are not uniform. The typical shear rate of each viscometer is given below:

$$\dot{\gamma} = \begin{cases} Pa/2\eta l & \text{(Panel a; at the capillary wall)} \\ 2a/3\upsilon & \text{(Panel b; at the equator of the ball)} \\ 2\Omega r_2^2 / (r_2^2 - r_1^2) & \text{(Panel c; at the inner cylinder surface)} \\ \Omega/\phi & \text{(Panel d)} \end{cases} \qquad (2.2)$$

As mentioned in the next section, Sect. 2.4, η may depend on $\dot{\gamma}$, and the shear rate dependence is most accurately measured by the corn-and-plate viscometer, where the shear rate is constant within the sample liquid.

2.3.2 Simple Shear Flow

Though we have mentioned various flow types used for rheometry, all the flow can be regarded locally as the simple shear flow, which is defined as the flow in the sliding parallel planes illustrated in Fig. 2.3. In what follows, we consider this simple shear flow. The rate of this flow can be specified by the shear rate $\dot{\gamma}$, the velocity V of the upper plane relative to the bottom place divided by the thickness d of the liquid between the two parallel planes.

Let us define the Cartesian coordinate system where the x and y axes are parallel to the flow direction and vertical to the sliding planes, respectively, and the z axis is
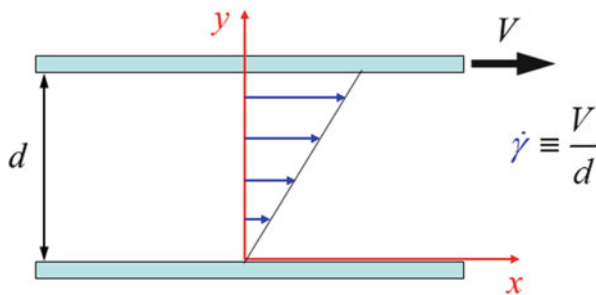

Fig. 2.3 Simple shear flow of the sample liquid sandwiched between the parallel plates

chosen to be vertical to both x and y axes to form the right-hand coordinate system (i.e., the upper side of the paper of Fig. 2.3 is chosen to be the positive z). Then, the velocity vector υ of the liquid can be written as

$$
\upsilon = \begin{pmatrix} \dot{\gamma}y \\ 0 \\ 0 \end{pmatrix} = \begin{pmatrix} 0 & \dot{\gamma} & 0 \\ 0 & 0 & 0 \\ 0 & 0 & 0 \end{pmatrix} \begin{pmatrix} x \\ y \\ z \end{pmatrix} = \left[\begin{pmatrix} 0 & \frac{1}{2}\dot{\gamma} & 0 \\ \frac{1}{2}\dot{\gamma} & 0 & 0 \\ 0 & 0 & 0 \end{pmatrix} + \begin{pmatrix} 0 & \frac{1}{2}\dot{\gamma} & 0 \\ -\frac{1}{2}\dot{\gamma} & 0 & 0 \\ 0 & 0 & 0 \end{pmatrix} \right] \begin{pmatrix} x \\ y \\ z \end{pmatrix}
$$

(2.3)

where the 3×3 matrix in the third side of the above equation is the shear rate matrix, which is divided into the two 3×3 matrices in the fourth side. As shown in Fig. 2.4, the two matrices in the fourth side represent the extension and rotation, respectively. Oppositely speaking, the simple shear flow consists of the vortex and rotation. We will discuss the effect of the rotation matrix on the polymer solution viscosity in the following.

To slide the upper plane by the velocity V, we need to apply the force F to the plane, and we define the shear stress σ by F/A where A is the area of the plane. The force is proportional to V, so that we can write

$$
\sigma \equiv \frac{F}{A} = \eta \frac{V}{d} = \eta \dot{\gamma}
$$

(2.4)

where η is the proportional constant and we have used the definition of $\dot{\gamma}$ in the last equation. This is the definition of the viscosity coefficient η. Since we apply the force F to the plane and the plane moves the distance V per unit time, we make the work FV per unit time to the flowing liquid. Using σ and $\dot{\gamma}$, we can write the work
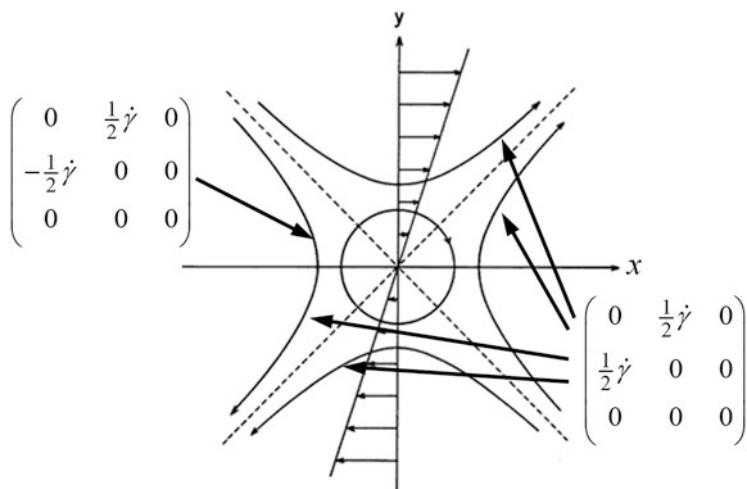

Fig. 2.4 Extensional and rotational components of the simple shear flow

w per unit time and unit volume in the form

$$w = \frac{FV}{Ad} = \sigma\dot{\gamma} = \eta\dot{\gamma}^2 \tag{2.5}$$

The last equation was obtained from Eq. 2.4.

2.4 Viscosity Coefficient

The viscosity coefficient η for a given polymer-solvent system depends on not only the shear rate $\dot{\gamma}$ of the flow, the temperature, and the pressure but also the polymer concentration c (the mass concentration with the units of g/cm^3) and the molecular weight M. Although we mostly deal with the c and M dependences in this chapter, we briefly mention the dependences on the shear rate and temperature.

If the shear rate of the solution flow is low enough, η is independent of $\dot{\gamma}$. This flow behavior is referred to as the Newtonian, and the viscosity coefficient at the low shear rate limit is called as the zero-shear viscosity. When the shear rate is increased in the rodlike and flexible polymer solutions, the orientation of rodlike polymer becomes anisotropic, and the conformation of the flexible polymer chain deforms from the thermally equilibrium one, respectively, in the solutions, which reduces the viscosity coefficient (the shear thinning effect). For aggregating polymer solutions, the shear flow may dissociate the aggregates, which also brings about the shear thinning effect. Although the shear thinning effect is important in some cases, we consider only the zero-shear viscosity in what follows.

The solvent viscosity strongly depends on the temperature. According to the hole theory of Cohen and Turnbull [5], the flow of the solvent composed of spherical particles occurs by the jump of the particle into a hole nearby, which is an activation process of a relatively high activation energy, leading to the strong temperature dependence. The conformation of the polymer chain is also dependent on the temperature, but its contribution to the temperature dependence of the solution viscosity is usually minor. If the heating dissociates polymer aggregates or thermal denaturation, the solution viscosity can reduce remarkably.

It is well known that the addition of the polymer to the solvent can increase remarkably the solution viscosity. For dilute polymer solutions, the c dependence of the zero-shear viscosity η is usually written as

$$\eta = \eta_s \left(1 + [\eta]\,c + k'[\eta]^2 c^2 + \cdots \right) \tag{2.6}$$

where η_s is the solvent zero-shear viscosity, $[\eta]$ is the intrinsic viscosity, and k' is the Huggins coefficient. The intrinsic viscosity $[\eta]$ is a measure of the ability of the viscosity enhancement of the polymer species, which we will consider theoretically later. The concentration dependence for the polymer solution viscosity is usually

so strong that terms with higher order than c^2 in Eq. 2.6 become important with increasing c.

The zero-shear viscosity also strongly depends on the molecular weight M of the solute polymer. Historically, the M dependence of the intrinsic viscosity $[\eta]$ has been important because one can determine M from $[\eta]$. The famous Mark-Houwink-Sakurada equation given by

$$[\eta] = KM^a \tag{2.7}$$

with two constants specific to the polymer-solvent system was proposed for this purpose. However, it should be noticed that this equation was originally proposed for flexible polymers and does not hold for stiff polymers over a wide M range. On the basis of the scaling concept [6, 7], many polymer solution properties in the semi-dilute regime can be expressed as a universal function of c/c^*, where c^* is the overlap concentration. Since c^* may be equated to the reciprocal of $[\eta]$, η_0 becomes a universal function of $c[\eta]$. Using Eq. 2.6, we can say that both c and M dependences of η_0 can be expressed as a function of $c[\eta]$. We should note again that the scaling concept was proposed for flexible polymer solutions, and it is questionable to apply the above argument to stiff polymer solutions.

2.5 Intrinsic Viscosity [2, 8]

2.5.1 Friction Between Polymer and Solvent

Let us calculate the intrinsic viscosity of a rodlike and flexible polymer chains composed by N beads of a diameter b suspended in the simple shear flow of the solvent (cf. Fig. 2.5). As mentioned in the previous section, the simple shear flow can be divided into the extension and rotation. At a sufficiently low shear rate, the former flow component does not affect the motion of the polymer chain, but the latter flow component rotates the polymer chain around the center of mass of the polymer chain with the angular velocity of $\dot{\gamma}/2$. (The center of mass itself moves along the x direction, but this motion does not contribute to η. We choose the center of mass as the origin of the Cartesian coordinate system and consider the relative motion of each bead to the center of mass.)

The simple shear flow behavior introduced in Sect. 3 does not depend on the z coordinate. Therefore, we omit the z component of vectors and matrices appearing in what follows, just for simplicity. The (relative) velocity υ_i of the i-th bead located at $\mathbf{r}_i = (x_i, y_i)$ and the (unperturbed) solvent flow velocity υ°_s at the same position are given by

$$\upsilon_i = \begin{pmatrix} 0 & \frac{1}{2}\dot{\gamma} \\ -\frac{1}{2}\dot{\gamma} & 0 \end{pmatrix} \mathbf{r}_i, \ \upsilon^\circ_s = \begin{pmatrix} 0 & \dot{\gamma} \\ 0 & 0 \end{pmatrix} \mathbf{r}_i \tag{2.8}$$
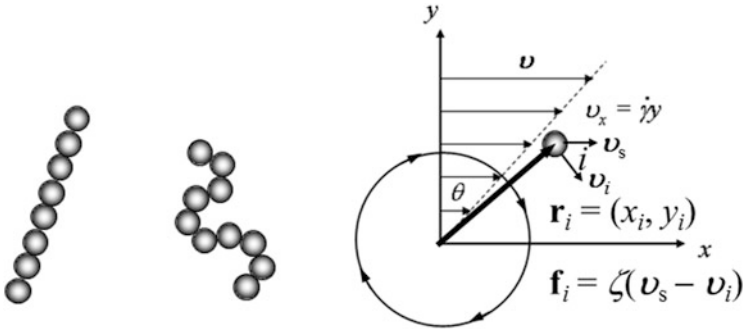
Fig. 2.5 Bead models for the rodlike polymer and the Gaussian chain and a bead under the simple shear flow

The difference between υ_i and $\upsilon^\circ{}_s$ produces the frictional force $\mathbf{f}_i = \zeta(\upsilon^\circ{}_s - \upsilon_i)$ $\mathbf{r}_i$, where $\zeta (=3\pi\eta_s b)$ is the frictional coefficient of the bead. The energy dissipation by this frictional force per unit time is given by $\mathbf{f}_i \cdot \upsilon^\circ{}_s$, and their sum over beads in a unit volume of the solution should be equal to w in Eq. 2.5 from the energy conservation rule, and we have the following relation:

$$w = \frac{cN_A}{M}\sum_{i=1}^{N}\mathbf{f}_i \cdot \upsilon^\circ{}_s = \frac{3\pi\eta_s bcN_A}{2M}\dot{\gamma}^2\sum_{i=1}^{N}y_i^2 \tag{2.9}$$

where N_A is the Avogadro constant and the prefactor cN_A/M is the number of polymer chains per unit volume of the solution. Combining this equation with Eq. 2.5, we obtain the molecular expression for the zero-shear viscosity induced by the friction between polymer and solvent (the viscous component of η) in the form

$$\eta_V = \frac{3\pi\eta_s bcN_A}{2M}\sum_{i=1}^{N}y_i^2 \tag{2.10}$$

In the above calculation of w, we did not consider the interchain hydrodynamic interaction, so that Eq. 2.10 should be applied to dilute solution where c^2 and the higher-order terms are neglected. Thus, the comparison between Eqs. 3.4.1 and 3.5.3 gives us the equation:

$$[\eta] = \frac{3\pi bN_A}{2M}\sum_{i=1}^{N}y_i^2 \tag{2.11}$$

Applying this equation to the rodlike polymer and the Gaussian chains, we obtain the following expressions:

$$[\eta] = \begin{cases} \frac{\pi N_A (bN)^3}{8M} & \text{(rodlike polymer)} \\ \frac{\pi N_A b^3 N^2}{12M} & \text{(Gaussian chain)} \end{cases} \qquad (2.12)$$

From the latter equation, it turns out that the exponent a in Eq. 2.7 is 1 for the Gaussian chain, which is the famous Staudinger equation for $[\eta]$. Ironically, Staudinger himself believed for a long time that all polymer chains are rodlike, but a for the rodlike polymer is 2 in Eq. 2.12, instead of his equation. Moreover, experimental M dependences of $[\eta]$ reported for many flexible polymer-solvent systems did not obey the Eq. 2.7 for the Gaussian chain.

2.5.2 Intramolecular Hydrodynamic Interaction

The above calculation, however, has not taken into account the perturbation of the solvent flow by motions of beads surrounding each bead. But actually this perturbation is important, and we have to modify Eq. 2.12 considering this effect. Figure 2.6 illustrates the solvent flow around the bead moving at the velocity υ by
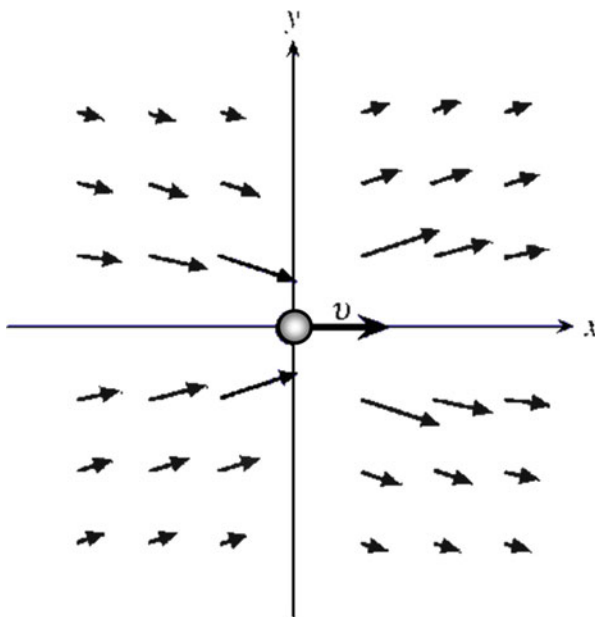

Fig. 2.6 Solvent flow field around a moving bead at the velocity υ in the x direction

the external force $\mathbf{F} = 3\pi \eta_s \upsilon$. Mathematically, the perturbation of the solvent flow υ'_s at the position $\mathbf{r}$ from the moving bead can be expressed by

$$\upsilon'_s = \mathbf{TF}, \quad \mathbf{T} \equiv \frac{1}{8\pi \eta_s r} \left(\mathbf{I} + \frac{\mathbf{rr}}{r^2} \right) \tag{2.13}$$

where $r \equiv |\mathbf{r}|$, $\mathbf{I}$ is the unit tensor, $\mathbf{rr}$ is the dyadic $[(\mathbf{rr})_{\alpha\beta} = \alpha\beta; \alpha, \beta = x, y, z]$, and $\mathbf{T}$ is called as the Oseen tensor. By this perturbation, the solvent flow velocity υ_s at the position of the i-th bead must be written as

$$\upsilon_s = \upsilon^\circ_s + \sum_{j \neq i} \upsilon'_{s,j} \tag{2.14}$$

instead of Eq. 2.8, where $\upsilon'_{s,j}$ is the perturbation by the j-th bead calculated by Eq. 2.13 with $\mathbf{r} = \mathbf{r}_i - \mathbf{r}_j$ ($\mathbf{r}_j$: the position vector of the j-th bead).

Using this equation for υ_s, Kirkwood and Riseman calculated $[\eta]$ for the rodlike polymer and the Gaussian chain both with sufficiently large N. Their results are written as

$$[\eta] = \begin{cases} \frac{\pi N_A L^3}{90M \ln(L/b)} & \text{(rodlike polymer)} \\ 6^{3/2} \Phi \frac{\langle S^2 \rangle^{3/2}}{M} & \text{(Gaussian chain)} \end{cases} \tag{2.15}$$

where L $(= bN)$ is the length of the rod, $\langle S^2 \rangle$ $(= b^2N/6)$ is the square radius of gyration of the Gaussian chain, and Φ is the Flory viscosity constant $(=2.87 \times 10^{23})$. The Mark-Houwink-Sakurada exponent a is 0.5 for the Gaussian chain, which agrees with experimental results. Compared with the Einstein viscosity equation for a hard sphere, it can be seen that the Gaussian chain with the radius of gyration of $\langle S^2 \rangle^{1/2}$ is equivalent to the sphere with the radius of $0.87\langle S^2 \rangle^{1/2}$, giving the same $[\eta]$. Because the solvent inside the Gaussian chain rotates together with the chain by the intramolecular hydrodynamic interaction, the Gaussian chain behaves like a sphere. The double logarithmic plot of $[\eta]$ against M for rodlike polymer follows a concave curve due to the factor $1/\ln(L/b)$ in Eq. 2.15, and the slope approaches ca. 1.7 at high M, which is also consistent with experimental results, as mentioned below. Thus, for the rodlike polymer, $[\eta]$ does not obey the Mark-Houwink-Sakurada equation.

2.5.3   Contribution of the Elastic Stress

It is well known that polymer molecules move and rotate randomly by thermal agitation in solution, but so far we have not taken into account this Brownian motion, which may contribute to the solution viscosity. When a stepwise shear deformation is exerted on the rodlike polymer solution, the extension component (cf. Eq. 2.2) of the very fast shear flow orients rods to the direction along the line $y = x$. After the

deformation, the shear flow is stopped and the orientation of the rods is randomized by the rotational diffusion. Thus, the stepwise deformation provides the transient orientational entropy loss. According to the theory of rubber elasticity, the entropy loss induces the force (or the stress) to recover the system to the original state before the deformation (the Le Chatelier principle), and the transient stress after the stepwise shear deformation is written as

$$\sigma = \frac{k_B T}{5} \frac{cN_A}{M} \exp\left(-2D_r t\right) \qquad (2.16)$$

for thin rods ($L \gg b$), where $k_B T$ is the Boltzmann constant multiplied by the absolute temperature, t is the time elapsing after the deformation, and D_r is the rotational diffusion coefficient of the rodlike polymer in the solution.

This stress relaxation followed by the stepwise deformation can be expressed by the Maxwell model consisting of an elastic spring with the spring constant k and a dashpot including a fluid of the viscosity coefficient η_d in a series, which writes the transient stress as

$$\sigma = k \exp\left(-t/\tau\right) \qquad (2.17)$$

where τ is the relaxation time given by η_d/k. Comparing Eqs. 2.16 and 2.17, we have the relations $k = (k_B T/5)(cN_A/M)$ and $\tau = 1/2D_r$. On the other hand, for the steady shear flow, the Maxwell model gives the equation for the shear stress as

$$\sigma = k\tau\dot{\gamma} \qquad (2.18)$$

Compared this equation with Eq. 2.3, the elastic component of the zero-shear viscosity η_E is related to D_r by

$$\eta_E = \frac{RTc}{10MD_r} \qquad (2.19)$$

with the gas constant R ($=k_B N_A$).

The hydrodynamic calculation gives us the rotational diffusion coefficient $D^\circ_{r,0}$ at infinite dilution in the form

$$D^\circ_{r,0} = \frac{3k_B T \ln(L/b)}{\pi \eta_s L^3} \qquad (2.20)$$

in the condition of $L \gg b$. By adding the elastic component to Eq. 2.15 of $[\eta]$ for the rod with $L \gg b$, we obtain the total intrinsic viscosity as

$$[\eta] = \frac{2\pi N_A L^3}{45M \ln(L/b)} \qquad (2.21)$$

The elastic component enlarges $[\eta]$ by the factor 4, but the M dependence does not change.

The Gaussian chain has a lot of internal degrees of freedom, and the micro-Brownian motion with respect to the degrees of freedom can be treated by using the bead-spring model where N beads are connected by $N-1$ elastic springs. Zimm calculated $[\eta]$ for the bead-spring model including the effect of the intramolecular hydrodynamic interaction and micro-Brownian motion. The result is given in the same form as the second line of Eq. 2.15, where Φ is written as

$$\Phi = \frac{\pi}{4}\sqrt{\frac{\pi}{3}}N_{\mathrm{A}}\sum_{j=1}^{N}\frac{1}{\lambda'_j} \tag{2.22}$$

where λ'_j is the eigenvalue of the transformation matrix into the normal coordinates. The numerical calculation of λ'_j gives us Φ to be 2.84×10^{23}, which is in a good agreement with Φ obtained by Kirkwood and Riseman (Eq. 2.15), but this agreement may be just by accident, because the two theories used the different polymer models. For the bead-spring model in solution, η cannot be divided into the viscous and elastic components. We can say from Eq. 2.22 that the normal mode $j = 1$, which approximately corresponds to the end-over-end rotation of the chain, contributes to η ca. 42 %.

2.5.4 Wormlike Chain Model and Excluded Volume Effect

Cellulose and its derivatives are known to be semiflexible polymers. The double-helical polysaccharide xanthan, triple-helical polysaccharide schizophyllan, and so on are typical stiff polymers. Their molecular conformation can be represented as the wormlike chain model, which interpolates between the Gaussian chain and rodlike polymer. This model is characterized by the contour length L and the persistence length q. The latter quantity is larger for the stiffer polymer. When this model is applied to a polysaccharide with the molecular weight M, we can calculate L by hM/M_0, where h and M_0 are the (average) contour length and molar mass per monosaccharide unit of the polysaccharide main chain, respectively. This model becomes identical with the Gaussian chain, if M tends to infinity. The parameters b and N of the Gaussian chain correspond to $2q$ and $N_{\mathrm{K}} \equiv L/2q$ of the wormlike chain, where $2q$ and N_{K} are sometimes referred to as the length and number of Kuhn's statistical segments, respectively. The radius of gyration of the wormlike chain is written as

$$\langle S^2 \rangle = (2q)^2 \left\{ \frac{1}{6}N_{\mathrm{K}} - \frac{1}{4} + \frac{1}{4N_{\mathrm{K}}}\left[1 - \frac{1}{2N_{\mathrm{K}}}\left(1 - e^{-2N_{\mathrm{K}}} \right) \right] \right\} \tag{2.23}$$

At low and high M limits, the above equation tends to

$$\langle S^2 \rangle = \begin{cases} \frac{1}{12}L^2 \ (M \to 0) \\ \frac{1}{6}(2q)^2 N_K \ (M \to \infty) \end{cases} \tag{2.24}$$

that is, the rod and Gaussian chain limits, respectively.

The intrinsic viscosity for the wormlike chain model (the wormlike cylinder or wormlike touched-bead model) was formulated by Yamakawa et al. The intrinsic viscosity equation is not given in a simple analytic equation but in a complex form of the empirical interpolation formulas. The molecular weight dependence of $[\eta]$ for the wormlike chain model obeys that for the rodlike polymer in the low M region and the Gaussian $M^{1/2}$ relation in the high M region. The double logarithmic plot of $[\eta]$ vs. M thus does not follow the Mark-Houwink-Sakurada equation.

Parts of a polymer chain cannot overlap, but the above equations for $\langle S^2 \rangle$ and $[\eta]$ of the wormlike chain do not consider this excluded volume effect. While this effect disappears at the rod limit because of no possibility of the self-interaction, it becomes important with increasing the chain flexibility. The excluded volume effect for the wormlike chain was considered also by Yamakawa et al. By this effect, the polymer chain expands, and the degree of the expansion is expressed in terms of the expansion factor α_S defined by the radius of gyration divided by the unperturbed one or α_η defined by $[\eta]^{1/3}$ divided by the unperturbed one. The strength of the excluded volume effect is characterized by the excluded volume strength B, and the expansion factors α_S and α_η are given as functions of $B/2q$ and N_K. When $B/2q$ or N_K increases from zero, the excluded volume effect becomes important, and α_S and α_η increase from unity. At the Gaussian chain limit ($N_K \to \infty$), α_S and α_η are proportional to $N_K^{1/10}$ in a good solvent, where the chain has a positive value of B, and $\langle S^2 \rangle^{1/2}$ and $[\eta]$ are proportional to $M^{0.6}$ and $M^{0.8}$, respectively.

2.6 Zero-Shear Viscosity at Finite Concentrations [3, 7]

2.6.1 Rodlike Polymer Solutions

As already mentioned above, the zero-shear viscosity of rodlike polymer solutions consists of the solvent, viscous, and elastic components:

$$\eta = \eta_s + \eta_V + \eta_E \tag{2.25}$$

The viscous component η_V is related to the rotational diffusion coefficient $D_{r,0}$ by

$$\eta_V = \frac{RTc}{30MD_{r,0}} \tag{2.26}$$
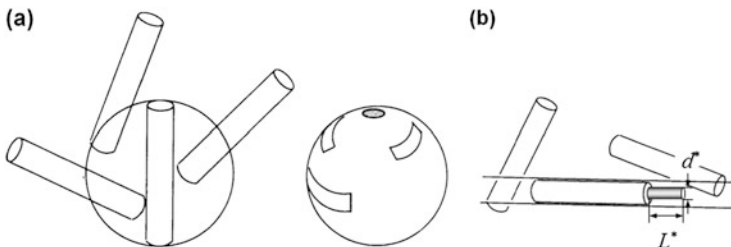
Fig. 2.7 Rods in a concentrated solution, where a rotating rod (**a**) or a longitudinally moving rod (**b**) collides with surrounding rods

From Eqs. 2.15 to 2.20, $D_{r,0} = D^{\circ}{}_{r,0}$ at the infinite dilution. With increasing the polymer concentration, the motion of surrounding rods perturbs the solvent flow at the rod taking into consideration, which affects the rotational diffusion coefficient, and then η_V. Although there are many hydrodynamic calculations, the long-range nature of the intermolecular hydrodynamic interaction makes mathematical calculations difficult, and rigorous calculation has not been performed yet. Here, the intermolecular hydrodynamic interaction is empirically expressed using an adjustable parameter k'_{HI}, and $D_{r,0}$ is written as

$$D_{r,0}{}^{-1} = D^{\circ}_{r,0}{}^{-1} \left(1 + k'_{HI} [\eta] c\right) \tag{2.27}$$

For the elastic component η_E, Eq. 2.19 holds even at finite polymer concentrations. The rotational motion of each rod is affected by surrounding rods at finite concentration through not only the intermolecular hydrodynamic interaction but also the direct collision among rods (cf. Fig. 2.7a). Because η_V arises from the friction between the polymer and solvent, we do not consider the effect of the direct collision, but we have to consider both effects on η_E through D_r.

2.6.2 Rotational Diffusion Coefficient and Viscosity Equation

As illustrated in Fig. 2.7a, the rotational diffusion motion of a rodlike polymer (enclosed by the circle in the figure) is hindered by the collision with surrounding rods in solution. This hindered rotational diffusion motion can be treated as the two-dimensional translational diffusion motion of a circular object on the spherical surface, where ribbonlike objects (the projection of the hindering rod onto the spherical surface) hinder the translational diffusion motion.

The collision effect on D_r, sometimes called as the entanglement effect, can be treated by the mean-field Green function method. Originally, this method was applied by Edwards and Evans to the longitudinal diffusion motion in the

concentrated rodlike polymer solution and then extended by Teraoka and Hayakawa to the transverse and rotational diffusion motions.

Although the rotational diffusion motion is two-dimensional, we briefly explain the mean-field Green function method for the one-dimensional diffusion motion of a particle. The extension to the rotational diffusion motion of a rod is straightforward, but mathematically more complex, which is the reason why we explain the method in the one dimension.

The diffusion motion is stochastic, so that we can discuss only the probability of the motion. Let x be the coordinate of the diffusing particle in its one-dimensional path. If no barriers are present in the path, the *unperturbed* conditional probability $G_0(x, x'; t, t')$ that the particle at the position x' at time t' moves to the position x at time t is given by

$$G_0\left(x, x'; t, t'\right) = \frac{1}{\sqrt{4\pi D_0\left(t - t'\right)}} \exp\left[-\frac{(x - x')^2}{4D_0\left(t - t'\right)}\right] \tag{2.28}$$

where D_0 is the unperturbed diffusion coefficient of the particle. Mathematically, this conditional probability is referred to as the Green function. Figure 2.8 illustrates functional forms of $G_0(x, x'; t, t')$ given by Eq. 2.28 at three different $t - t'$. If one drops ink in water at x', ink diffuses and the concentration distribution of ink changes with time according to the functional forms in the figure.
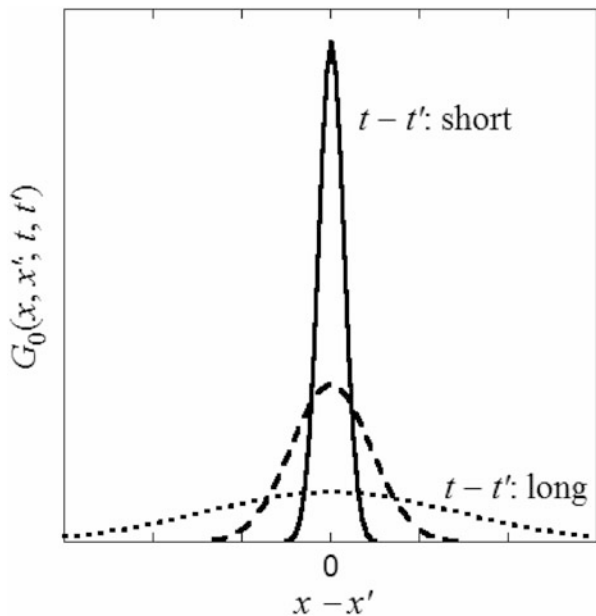

Fig. 2.8 Unperturbed Green function (the conditional probability) of the one-dimensionally diffusing particle

Suppose now a single reflecting point barrier is placed at position R in the path at time t_R and removed at time t_Q. Following Edwards and Evans, the Green function perturbed by this barrier can be expressed by

$$G\left(x, x'; t, t'\right) = \int_{-\infty}^{\infty} dx_1 \int_{-\infty}^{\infty} dx_2 G_0\left(x, x_2; t, t_Q\right) Q'\left(x_2, x_1; t_Q, t_R\right) G_0\left(x_1, x'; t_R, t'\right) \tag{2.29}$$

where $Q'(x_2, x_1; t_Q, t_R)$ is the transition probability that the particle at the position x_1 at time t_R moves to the position x_2 at time t_Q. After averaging the Fourier transform of Eq. 2.29 with respect to the random variables R, t_R, and t_Q, and making some mathematical manipulations, we obtain

$$\left\langle \widehat{G}\left(k; t, t'\right) \right\rangle \equiv \int_{-\infty}^{\infty} G\left(x, x'; t, t'\right) e^{ik(x-x')} d\left(x - x'\right) = e^{-D_0(t-t')k^2} + \left\langle \Delta\widehat{G}\left(k; t, t'\right) \right\rangle \tag{2.30}$$

with the perturbed part $\langle \Delta\hat{G}(k; t, t') \rangle$ given by

$$\left\langle \Delta\widehat{G}\left(k; t, t'\right) \right\rangle = \frac{8}{3\sqrt{\pi}l}(D_0\tau)^{3/2}k^2 + O\left(k^4\right) \tag{2.31}$$

for a sufficiently long time interval $t - t'$. Here, l is a path length comparable to the maximum distance that the particle can diffuse during $t - t'$, and τ is the mean lifetime of the barrier. The brackets $\langle \cdots \rangle$ represent the average with respect to R, t_R, and t_Q. The effective diffusion coefficient D can be calculated from

$$D = -\lim_{t-t'\to\infty} \frac{1}{2\left(t - t'\right)} \frac{\partial^2 \left\langle \widehat{G}\left(k; t, t'\right) \right\rangle}{\partial k^2}\Bigg|_{k=0} \tag{2.32}$$

From Eqs. 2.31 to 2.32, we get D in the presence of a single reflecting barrier as

$$D = D_0 - \frac{8(D_0\tau)^{3/2}}{3\sqrt{\pi}l\left(t - t'\right)} \tag{2.33}$$

Next, we consider the case where more than one barrier appears in the diffusion path, and particle receives multiple perturbations. Teraoka and Hayakawa assumed that the Green function for this case satisfies the following Dyson equation:

$$\langle G \rangle = G_0 + G_0 \left\langle \sum_{i=1}^{M} Q_i \right\rangle \langle G \rangle \tag{2.34}$$

where Q_i is the i-th perturbation element and M is the number of elements appearing on the path length l between t and t'. In Eq. 2.34, we have omitted the arguments of

the Green functions and Q_i as well as the integral symbol; the second term on the right-hand side of Eq. 2.34 involves the same integration as in Eq. 2.29. When the whole right-hand side is inserted into $\langle G \rangle$ on the right- hand side, it turns out that Eq. 2.34 gives a Green function perturbed by any number of sequential independent elements. Eq. 2.34 can be solved recursively, and the Fourier transform of the solved $\langle G \rangle$ is inserted into Eq. 2.32 to obtain

$$D = D_0 \left(1 + \frac{4}{3\sqrt{\pi}} \rho_B \tau^{3/2} D_0^{1/2} \right)^{-2} \tag{2.35}$$

where $\rho_B \ [\equiv M/l(t - t')]$ is the number of the barriers appearing per unit path length and unit time. If only a barrier appears for a sufficiently long time interval $t - t'$, Eq. 2.35 reduces to Eq. 2.33 for the first-order perturbation.

We can extend the above theory to the two-dimensional rotational diffusion motion. The perturbed rotational diffusion coefficient D_r can be written as

$$D_r = D_{r,0} \left[1 + \sqrt{\frac{6}{\beta}} \frac{N_A c L^3}{M} \left(\frac{D_{\|,0}}{D_\|} \right)^{1/2} \right]^{-2} \tag{2.36}$$

where β is a constant and $D_\|$ is the perturbed longitudinal diffusion coefficients of the rod. To obtain this equation, we have assumed $\tau \propto L^2/D_\|$, because the hindrance of the rotational motion by surrounding rods is released mainly through the longitudinal motion of the hindering or rotating rod. Teraoka calculated β to be 1350 by simulation for entangled rods.

We need an equation for $D_\|$ to calculate D_r from Eq. 2.36. Edwards and Evans formulated $D_\|$ by the mean-field Green function method, but their equation can be only applied to very concentrated solutions of rodlike polymers, where the transverse motion of each rod is almost completely prohibited. We want to formulate the viscosity equation for rodlike polymers in less concentrated solutions. Sato and Teramoto proposed to formulate $D_\|$ by the hole theory. This method is similar to that used by Cohen and Turnbull to obtain an expression of the self-diffusion coefficient in liquids of small molecules and metals. The basic assumption in our hole theory is that the longitudinal diffusion of a test chain occurs only when a "hole" that is larger than a critical hole exists in front of the test chain. Here the hole means a region that contains no chain segments in the solution (not true vacuum region), and then one should not confuse that with the free volume that often appears in the literature on polymer melts and solutions.

From Cohen and Turnbull's argument [5], it turns out that $D_\|$ is proportional to the total probability P_h of finding a hole that is larger than the critical hole. The probability P_h is written in terms of the average mutual excluded volume V_{ex}^* between the critical hole and the solute molecule as

$$P_h = \exp \left(-V_{ex}^* c' \right) \tag{2.37}$$

and thus $D_\parallel$ is given by

$$D_\parallel = D_{\parallel,0} \exp\left(-V_{\text{ex}}{}^* c'\right) \tag{2.38}$$

When the critical hole for the rodlike polymer with the length L and diameter d is assumed to be a cylinder of the length $L^* = \lambda^* L$ and diameter $d^* = \lambda^* d$, where λ^* is the constant similitude ratio (cf. Fig. 2.7b), $V_{\text{ex}}{}^*$ is written as

$$V_{\text{ex}}{}^* = \tfrac{\pi}{4}\Big[LL^*(d + d^*) + Ld^2 + L^* d^{*2} + \tfrac{1}{2}\left(Ld^{*2} + L^* d^2\right) + \tfrac{\pi}{2}(L + L^*)\,dd^* \\ + \tfrac{\pi}{4}(d + d^*)\,dd^* \Big] \tag{2.39}$$

Combining all the results (Eqs. 2.25–2.27, 2.19, 2.36, and 2.38), we obtain the viscosity equation for rodlike polymer solutions:

$$\frac{\eta - \eta_s}{\eta_s} = [\eta]\,c\left(1 + k'_{\text{HI}}\,[\eta]\,c\right)\left\{ \frac{1}{4} + \frac{3}{4}\left[1 + \sqrt{\frac{6}{\beta}\frac{N_A c L^3}{M}}\exp\left(\frac{1}{2}V_{\text{ex}}{}^* c'\right)\right]^2 \right\} \tag{2.40}$$

Expanding the above equation in the power series of c and comparing the second-order term with Eq. 2.6, we can express the Huggins coefficient k' in the form

$$k' = k'_{\text{HI}} + k'_{\text{EI}} \tag{2.41}$$

where k'_{EI} is the contribution of the entanglement interaction to k', given by

$$k'_{\text{EI}} = \frac{135}{4\pi\sqrt{\beta}}\ln\left(L/b\right) \tag{2.42}$$

On the other hand, the contribution k'_{HI} of the hydrodynamic interaction for rodlike polymer solutions has formulated by Riseman and Ullman. However, their calculation contains an improper integration, and thus the results are not conclusive.

When both hydrodynamic interaction and the concentration dependence of $D_\parallel$ are neglected in Eq. 2.40, η of the rodlike polymer solution at high concentrations depends on the molecular weight and concentration as $\eta \propto c^3 M^6/\ln(L/b)$. These dependences were predicted by Doi and Edwards [7]. However, these M and c dependences are modified by the effects of the hydrodynamic interaction and the concentration dependence of $D_\parallel$. If the effect of the hydrodynamic interaction is taken into account, η depends on M and c as $\eta \propto c^4 M^8/\ln^2(L/b)$ at high concentrations.
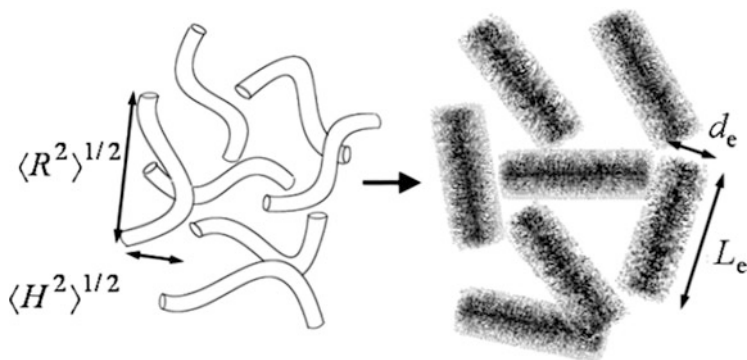
Fig. 2.9 Fuzzy cylinder model for semiflexible polymers in a concentrated solution

2.6.3 Flexibility and Finite Thickness Effects

The left illustration of Fig. 2.9 depicts semiflexible polymers in an isotropic concentrated solution. Each polymer chain rotates, translates, and changes its conformation in the solution. Among those molecular motions, the conformational change is rapidest, which smears the segment distribution as shown in the right illustration of Fig. 2.9. To formulate D_r of the semiflexible polymer in a concentrated solution, we view the polymer chain as this smeared cylindrical segment distribution, called as the fuzzy cylinder. The effective length L_e and diameter d_e of the fuzzy cylinder are defined using the mean square end-to-end distance $\langle R^2 \rangle$ and mean square distance $\langle H^2 \rangle$ between the midpoint and the end-to-end axis of the wormlike chain by

$$L_e = \langle R^2 \rangle^{1/2}, d_e = \left(\langle H^2 \rangle + b^2 \right)^{1/2} \qquad (2.43)$$

where b is the thickness of the wormlike chain polymer. Both $\langle R^2 \rangle$ and $\langle H^2 \rangle$ can be calculated from q and N_K of the wormlike chain; $L_e = L$ and $d_e = b$ in the rod limit, and $L_e = 6^{1/2} d_e$ in the Gaussian coil limit. (Strictly speaking, $\langle H^2 \rangle$ has not been formulated for the wormlike chain, but for the Tagami model, allowing the chain contour to stretch in contrast to the wormlike chain. However, the Tagami model provides the identical expressions of $\langle R^2 \rangle$ and $\langle S^2 \rangle$, so that we can expect its $\langle H^2 \rangle$ is a good approximation of that for the wormlike chain.)

Using the fuzzy cylinder model, we may extend the viscosity equation for the rodlike polymer solution in the previous subsection to semiflexible one by replacing L with L_e. However, we have to consider the finite thickness effect on the viscosity equation, because the axial ratio L_e/d_e of the fuzzy cylinder decreases with increasing the chain flexibility. The extension of Eq. 2.36 for D_r to the fuzzy

cylinder system can be written as

$$\frac{D_r}{D_{r0}} = \left[1 + \sqrt{\frac{6}{\beta} \frac{N_A c L_e^4}{ML}} F \left(\frac{D_{\parallel,0}}{D_\parallel}\right)^{1/2}\right]^{-2} \tag{2.44}$$

where F is a factor relating to the finite thickness effect, empirically given by

$$F \equiv \left(1 + C_r \frac{d_e}{L_e}\right)^3 \left(1 - C_r \frac{d_e}{5L_e}\right), \quad C_r = \frac{1}{2}\left[\tanh\left(\frac{1}{4}N_K - 1\right) + 1\right] \tag{2.45}$$

The final viscosity equation for semiflexible polymer solutions at finite concentration is given by

$$\frac{\eta - \eta_s}{\eta_s} = [\eta]\,c\,(1 + k'_{HI}\,[\eta]\,c) \left\{\frac{1}{4} + \frac{3}{4}\left[1 + \sqrt{\frac{6}{\beta}\frac{N_A c L_e^4}{ML}} F \exp\left(\frac{1}{2}V_{ex}^* c'\right)\right]^2\right\} \tag{2.46}$$

instead of Eq. 2.40. Here, V_{ex}^* is calculated by Eq. 2.39, using $L^* = \lambda^* L_e$ and diameter $d^* = \lambda^* d_e$. (Sato et al. further extended the viscosity equation, including the finite thickness effect of the polymer chain on frictional properties, but this effect is not important if $L \gg b$.)

Expanding the above equation in the power series of c, we have the expression for the Huggins coefficient k' as the sum of the contributions of the entanglement and hydrodynamic interactions as in Eq. 2.41. The contribution k'_{EI} of the entanglement interaction to k' is given by

$$k'_{EI} = \frac{3}{2}\sqrt{\frac{6}{\beta}\frac{N_A L_e^4}{[\eta]\,ML}} F \tag{2.47}$$

instead of Eq. 2.42.

When the concentration dependence of $D_\parallel$ is neglected in Eq. 2.46, the polymer concentration dependence η at high concentrations is not affected by the chain flexibility, i.e., $\eta \propto c^3$ and c^4, when the hydrodynamic interaction is neglected and not neglected, respectively. The molecular weight dependence of η for semiflexible polymer solutions does not obey any power law, because the polymer chain conformation changes from the rodlike to random coil with increasing M. In the coil limit, both L_e and $[\eta]$ are proportional to $M^{1/2}$ (without considering the excluded volume effect); Eq. 2.46 at $V_{ex}^* = 0$ gives us the relation $\eta \propto M^{1/2}$ and M in the dilute and concentrated limits, respectively. The dependence in the concentrated limit is very much different from the M dependence of η for the rodlike polymer solution, mentioned in the previous subsection [$\eta \propto M^8/\ln^2(L/b)$]. It is noted however that when the polymer concentration is high enough, the fuzzy cylinder model becomes

inappropriate, and we have to consider the reptation-like motion of the flexible chain in the entangled polymer network. We expect the well-known relation, $\eta \propto M^{3.4}$, for very concentrated flexible polymer solutions.

2.7 Comparison with Experimental Polymer Solution Viscosities [9]

2.7.1 Polymers with Different Chain Stiffness

While most of synthetic polymers are flexible, except for conjugated polymers, e.g., polyacetylenes and aromatic polyamides, biopolymers have a variety of the chain stiffness. Here, since we are mostly interested in the chain stiffness effect on the polymer solution viscosity, we show experimental solution viscosity data of different chain stiffness polymers shown in Fig. 2.10. In the figure, schizophyllan (SPG) is an extracellular polysaccharide produced by a fungus *Schizophyllum commune*. This polysaccharide forms a rigid triple helix in aqueous solution, which is one of the stiffest polymers we know so far. Xanthan is a bacterial polysaccharide produced by the *Xanthomonas campestris*, which forms a stiff double helix in aqueous salt solution. Cellulose is known to be a semiflexible polymer, and cellulose
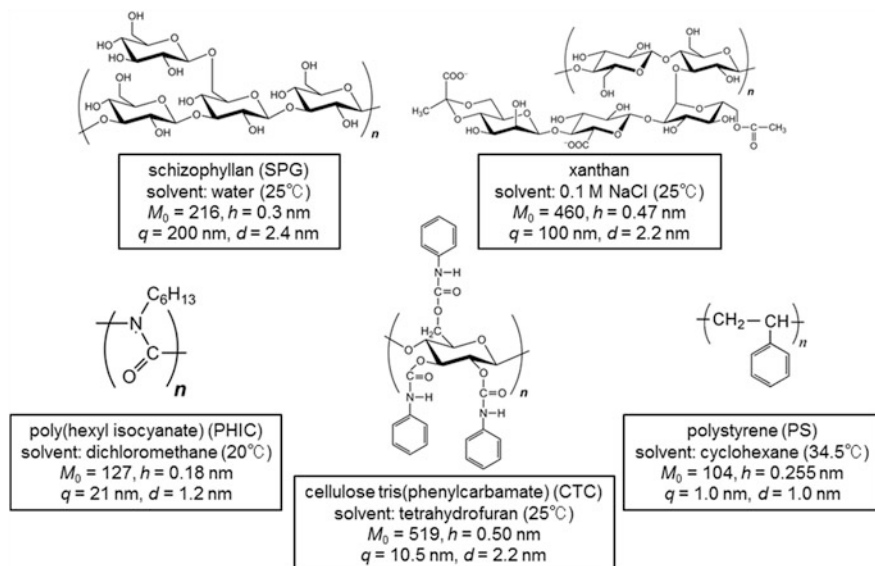

Fig. 2.10 Chemical structures and molecular characteristics of polymers with different chain stiffness

tri(phenylcarbamate) (CTC) is its derivative dissolved in organic solvents, say, tetrahydrofuran (THF).

The chain stiffness of those polysaccharides (and the derivative) is represented in terms of the persistence length q, which is listed in Fig. 2.10, as well as other molecular parameters, the molar mass M_0 and contour length h per glucose residue, and the diameter or thickness of the polymer chain d. While the values of M_0 and h were determined from the chemical structure, q was estimated from the molecular weight dependence of the radius of gyration or of the hydrodynamic properties (the hydrodynamic radius, sedimentation coefficient, or intrinsic viscosity). The diameter d may be calculated from both the partial specific volume of the polymer and the hydrodynamic properties. The d values estimated from the latter are sometimes slightly larger than those from the former. To fill up the gap between q of xanthan and CTC, I add a synthetic polymer, poly(hexyl isocyanate) (PHIC), which is a main-chain conjugated polymer with $q = 21$ nm in dichloromethane (DCM). Furthermore, I add also polystyrene (PS) as the typical flexible polymer, to examine the chain stiffness effect on the polymer solution viscosity. The molecular parameters were determined in the same way.

The intramolecular excluded volume effect for PS does not play any role in the theta solvent cyclohexane (CH). Furthermore, the same effect is also not important for stiff polymers because of the scarce probability of the self-interaction. Only the excluded volume effect of CTC in the good solvent THF may be appreciable at high molecular weights.

2.7.2   Dilute Region

As already shown in Fig. 2.1 for aqueous NaCl solutions of xanthan, the polymer concentration dependence of the zero-shear viscosity η strongly depends on the polymer molecular weight. Figure 2.11 illustrates the concentration dependences in a dilute region in the form of the linear plot.

From the initial slope, one obtains the intrinsic viscosity $[\eta]$ (cf. Eq. 2.6), but $[\eta]$ are usually determined by the use of the Huggins plot, $[(\eta/\eta_s) - 1]/c$ vs. c, or the Mead-Fuoss plot, $[\ln (\eta/\eta_s) - 1]/c$ vs. c, although those plots are not shown in Fig. 2.11. The molecular weight dependence of $[\eta]$ for xanthan in 0.1 M aqueous NaCl is shown in Fig. 2.12a, along with the results of the other four polymers in dilute solution. In the abscissa, M_w is the weight-average molecular weight. Data points for PS in cyclohexane obey the straight line with the slope of 0.5 in the double logarithmic plot, which agrees with the prediction of Eqs. 2.15 and 2.24 for the Gaussian chain. On the other hand, data points for the other stiffer polymers follow convex curves, not obeying the Mark-Houwink-Sakurada equation (Eq. 2.7) with constant K and a over the whole M_w ranges investigated. The curves for xanthan and SPG at $M_w < 5 \times 10^5$ have a slope of 1.6, which indicates that the xanthan double helix and SPG triple helix exist as rigid rods (cf. Eq. 2.15) in the M_w region. However, data points at the higher M_w follow the convex curves with smaller slopes,
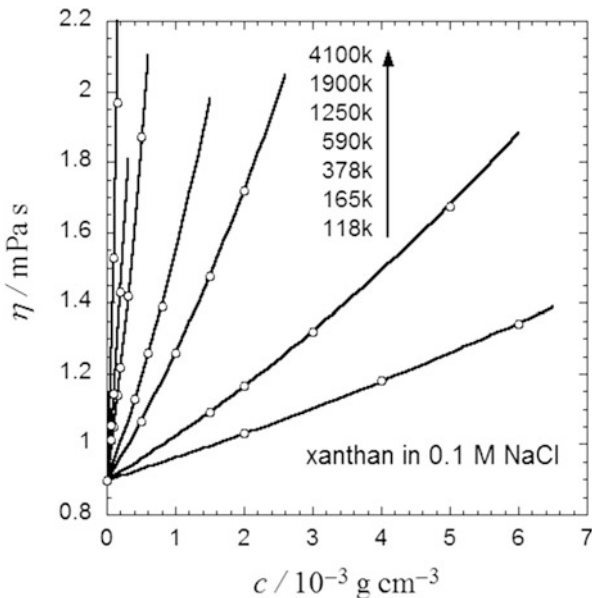
Fig. 2.11 Linear plots of the concentration c dependence of η for 0.1 M aqueous NaCl solutions of xanthan double helices with different molecular weights
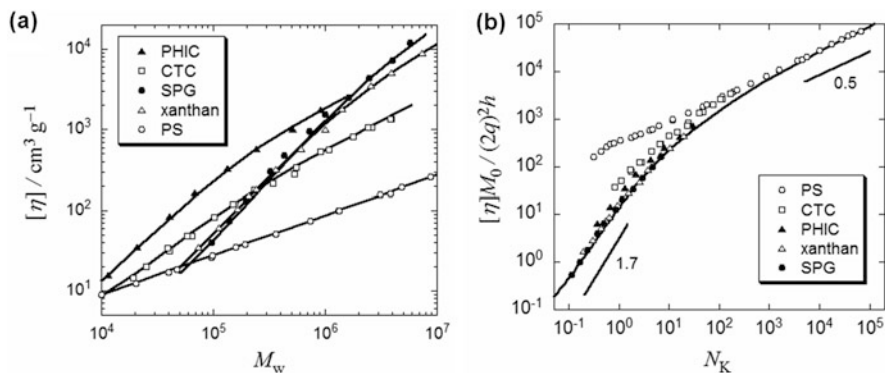

Fig. 2.12 Molecular weight dependence of $[\eta]$ for the five polymers; (**a**) plots of $[\eta]$ against M_w with theoretical curves (*solid curves*) calculated by the wormlike chain model using the parameters listed in Fig. 2.10; (**b**) universal plots of $[\eta]M_0/(2q)^2h$ against $N_K \equiv M_w/[2q(M_0/h)]$ with theoretical curve (*solid curve*) calculated by the wormlike chain model for SPG

which reflect the flexibility of the helices. The curves for CTC and PHIC have slopes of 1.0 and 1.3 at $M_w < 10^5$, respectively, slightly smaller than that for xanthan and SPG, and the slopes decrease with increasing M_w. The slopes at the highest M_w are 0.85 (PHIC) and 0.7 (CTC), which are close to the slope (0.5) for PS in cyclohexane.

Figure 2.12b replots the $[\eta]$ data for the five polymers in the form of $[\eta]M_0/(2q)^2h$ vs. $N_K \equiv M_w/[2q(M_0/h)]$ (the number of Kuhn's statistical segments). All the data points except for PS at low M_w almost obey a single composite curve (the solid curve) with slopes of 1.7 at low N_K (for the rod limit) and 0.5 at higher N_K (for the Gaussian limit). Deviations of data points for PS and CTC in low M_w regions from the composite curve come from the finite thickness effect on $[\eta]$. Because this effect is not important at sufficiently large axial ratio L/b, all the data points (except for CTC) approach to the composite curve in the high N_K region. Deviations of data points for CTC in high M_w region are due to the excluded volume effect.

From the curvature in the plot of η vs. c as shown in Fig. 2.11 or from the initial slope of the Huggins or Mead-Fuoss plots, we can determine the Huggins coefficient k'. The results for the five polymers are shown in Fig. 2.13a. Most of the data of k' are in between 0.3 and 0.5, irrespective of M_w and the chain stiffness. Therefore, k' is sometimes called as the Huggins constant, although it is not a constant, strictly speaking. Data of k' for PS at low M_w exceed 0.5 slightly.

According to Eq. 2.41, k' can be divided into the contributions of the entanglement and hydrodynamic interactions. The latter contribution k'_{EI} is calculated by Eq. 2.47, but the former contribution k'_{HI} cannot be calculated theoretically. Figure 2.13b shows k'_{EI} calculated by Eq. 2.47 for the five polymers by solid curves, and k'_{HI} estimated by subtracting k'_{HI} from the experimental k' in Panel a by symbols, as functions of N_K. (The theoretical values of k'_{EI} include the finite thickness effect of the polymer chain, which is neglected in Eq. 2.47.)

For stiff polymers, k'_{EI} exhibits a broad peak around $N_K = 1-10$. The peak shifts to larger N_K, and the peak height decreases with increasing the flexibility. On the other hand, k'_{HI}, except for PS, shows a broad minimum in the same N_K region and increases monotonically with N_K at large N_K, obeying a common asymptotic line. The deviation from the common line starts at larger N_K for more flexible polymers. When k'_{EI} and k'_{EI} for the same polymer are compared, k'_{EI} is superior to k'_{HI} for
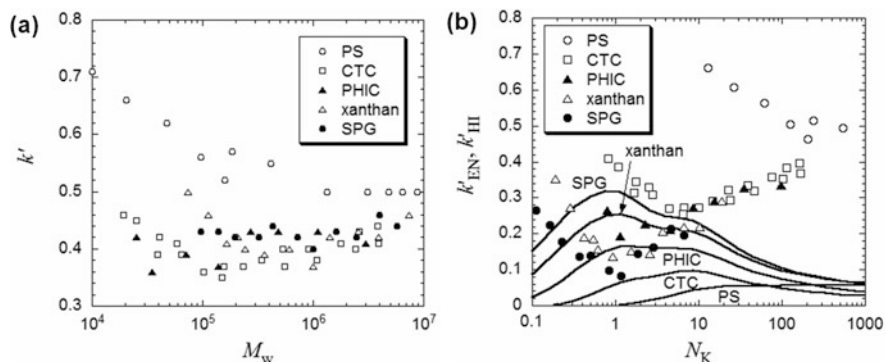

Fig. 2.13 (**a**) Molecular weight dependence of the Huggins coefficient k' and (**b**) contributions to the Huggins coefficient of the entanglement interaction k'_{EI} (*solid curves*) and of the hydrodynamic interaction k'_{HI} (*symbols*) for the five polymers

SPG and xanthan, they are comparable for PHIC, and k'_{HI} is predominant for CTC in the peak region. The hydrodynamic interaction term is much larger for PS over the entire N_K region.

2.7.3 Zero-Shear Viscosity Over a Wide Concentration Range

Figure 2.14a shows the concentration dependence of η for aqueous solution of seven schizophyllan (SPG) samples with different molecular weights, from 128 k ($=1.28 \times 10^5$) to 4300 k ($=4.3 \times 10^6$), over a wide concentration range. (Numbers in the parentheses in Fig. 2.14a indicate N_K values of the samples.) Solid curves in the figure indicate theoretical values calculated by Eq. 2.46 derived for the fuzzy cylinder model. In the equation, parameters L_e, d_e, L, and $[\eta]$ were estimated from the wormlike chain parameters listed in Fig. 2.10, and strengths of the hydrodynamic interaction k'_{HI} were estimated by subtracting k'_{HI} calculated by Eq. 2.47 (cf. Fig. 2.13b) from the experimental k'. Thus, the unknown parameter in Eq. 2.46 is only λ^* in V_{ex}^* (cf. Eq. 2.39). When λ^* is chosen to be 0.04, the theoretical curves nicely fit the experimental data points.

The contribution of V_{ex}^* or the effect of the concentration dependence of $D_{||}$ is not however so important, as demonstrated by dotted curves in Fig. 2.14b. Because this contribution becomes important exponentially with c, we might expect the importance at higher c. But the SPG solutions form a liquid crystal phase at high c, of which viscosity cannot be described by Eq. 2.46. We can say that the effect of the
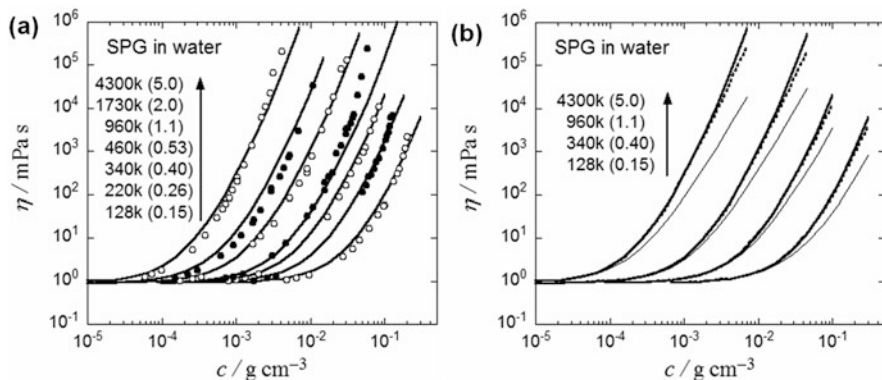

Fig. 2.14 (**a**) Concentration dependence of η for aqueous solutions of seven schizophyllan (SPG) samples with different molecular weights (N_K in the *parentheses*) along with *theoretical curves* calculated by Eq. 2.46; *dotted* and *thin solid curves* in Panel (**b**), calculated by Eq. 2.46 with $V_{ex}^* = \lambda^* = 0$ and with $V_{ex}^* = \lambda^* = k'_{HI} = 0$, respectively; *thick solid* curves in Panel (**b**) are the same as the solid curves in Panel (**a**) calculated by Eq. 2.46 with $\lambda^* = 0.04$ and k'_{HI} given in Fig. 2.13b

concentration dependence of $D_\parallel$ (the so-called jamming effect) is not important in η for SPG isotropic solutions.

Figure 2.14b also displays thin solid curves calculated by Eq. 2.46 with $V_{ex}^* = \lambda^* = k'_{HI} = 0$. These curves deviate remarkably downward, indicating that the effect of the hydrodynamic interaction plays an important role in η at high c. Equation 2.46 predicts c^4 and c^3 dependences of η for the dotted and thin solid curves, respectively, in the high c region. The actual concentration dependence is slightly stronger than the c^4 dependence, because of the jamming effect.

Comparisons between theory and experiment for the solution viscosity of the remaining four polymers are shown in Fig. 2.15. The solid curves in each Panel are the theoretical curves calculated by Eq. 2.46 in the same way as in Fig. 2.14a. It is noted that there are no adjustable parameters in Eq. 2.46, if we select the same value for λ^* as in the case of SPG (=0.04). The agreement between the theory and experiment is good except for the highest M sample of PHIC ($N_K \sim 100$), the lowest M sample of CTC ($L/b < 10$), as well as all the samples of PS ($N_K > 50$). We can say
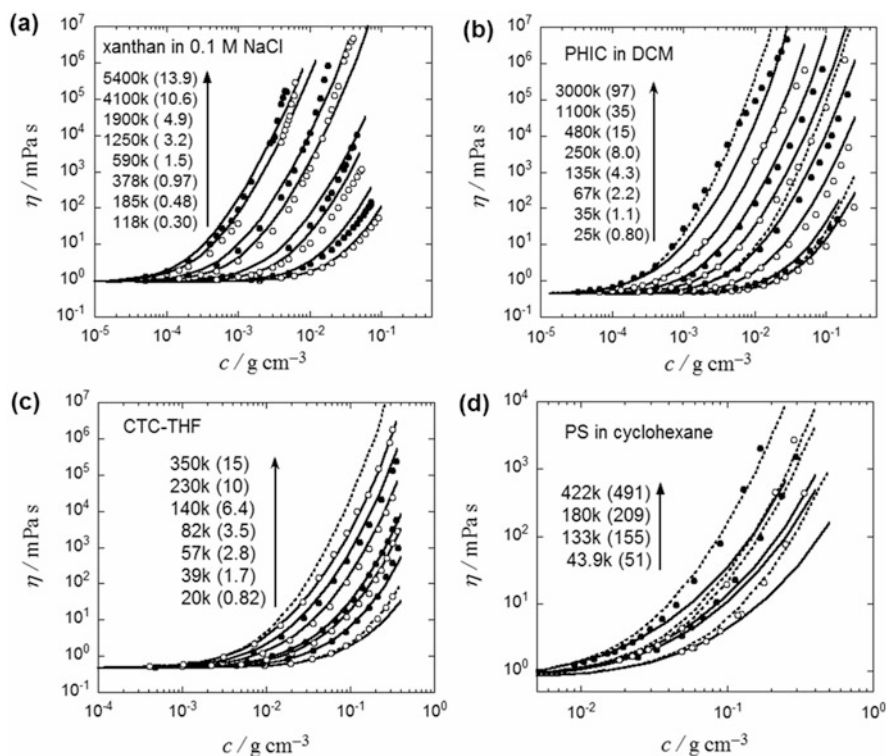

Fig. 2.15 Comparisons between theory and experiment for η of xanthan, PHIC, CTC, and PS solutions with different polymer molecular weights over wide concentration ranges; *solid curves* in each Panel, calculated by Eq. 2.46 with $\lambda^* = 0.04$ and k'_{HI} given in Fig. 2.13b; *dotted curves*, calculated by Eq. 2.48

that the viscosity equation (Eq. 2.46) predicts quantitatively the polymer solution viscosity if N_K <50 and L/b >10.

As indicated in Fig. 2.13b, the hydrodynamic interaction is more important in the Huggins coefficient than the entanglement interaction at N_K >50. In Eq. 2.46, the effect of the hydrodynamic interaction is considered only up to the linear order of c (cf. Eq. 2.27), but the higher-order term may be important at N_K >50. Beenakker [10] calculated η for spherical particle solutions up to the order of c^3. Applying his result to consider the higher-order effect of the hydrodynamic interaction, we modify Eq. 2.46 by

$$
\begin{aligned}
\frac{\eta - \eta_s}{\eta_s} = {}& [\eta]\, c \left(1 + k'_{HI}\, [\eta]\, c + \left(k'_{HI}\, [\eta]\, c \right)^2 \right) \\
& \times \left\{ \tfrac{1}{4} + \tfrac{3}{4} \left[1 + \sqrt{\tfrac{6}{\beta} \tfrac{N_A c L_e{}^4}{ML}} F \exp\left(\tfrac{1}{2} V_{ex}{}^* c' \right) \right]^2 \right\}
\end{aligned}
\tag{2.48}
$$

The dotted curves in Fig. 2.15 (Panels b–d) indicate theoretical values of η calculated by Eq. 2.48. The agreement between theory and experiment is improved by the modification for PHIC with $N_K = 97$ at intermediate c (Panel b) and for PS with $N_K > 50$ (Panel d). However, data points for PHIC with $N_K = 97$ at high c and with $N_K = 4.3$ and 0.80 in the whole c range (Panel b) are closer to the solid curve, indicating that the original Eq. 2.46 is better. In Panel c, data points for CTC with $N_K = 15$ are fitted to the solid curve, but data points with $N_K = 0.82$ and $L/b = 7.8$ to the dotted curve. From these comparison, we can say that the modified Eq. 2.48 improves the agreement with experimental data with N_K >50 and L/b <10, but not otherwise. The hydrodynamic interaction affects the polymer solution viscosity delicately, depending on the stiffness and the axial ratio of the polymer chain.

The viscosity equation Eq. 2.46 or 2.48 possesses two factors originated from the hydrodynamic interaction Λ_{HI} and the entanglement interaction Λ_{EI}, defined by

$$
\begin{cases}
\Lambda_{HI} \equiv 1 + k'_{HI}\, [\eta]\, c \ \text{or}\ 1 + k'_{HI}\, [\eta]\, c + \left(k'_{HI}\, [\eta]\, c \right)^2 \\
\Lambda_{EI} \equiv \tfrac{1}{4} + \tfrac{3}{4} \left[1 + \sqrt{\tfrac{6}{\beta} \tfrac{N_A c L_e{}^4}{ML}} F \exp\left(\tfrac{1}{2} V_{ex}{}^* c' \right) \right]^2
\end{cases}
\tag{2.49}
$$

Figure 2.16 shows the ratio $\Lambda_{HI}/\Lambda_{EI}$ for SPG (solid curves), PHIC (dot-dash curve), CTC (dotted curves), and PS (dashed curves). For stiff polymers, SPG and PHIC, the factor Λ_{EI} is superior to the factor Λ_{HI} at high concentrations. Although not shown in the figure, Λ_{EI} is predominant also for PHIC with higher M as well as for xanthan over the entire M. On the other hand, for the flexible polymer PS, the factor Λ_{HI} is superior to the factor Λ_{EI} at high concentrations. For the semiflexible polymer CTC with an intermediate chain stiffness, the importance of the two interactions depends on the molecular weight; Λ_{HI} is more important at low M but Λ_{EI} is more important at higher M. In Fig. 2.13b, we can see that $k'_{HI} > k'_{EI}$ for PHIC, CTC, and PS over the entire N_K (or M). Therefore, the predominance of the entanglement interaction is enhanced in solution viscosity at higher concentrations.
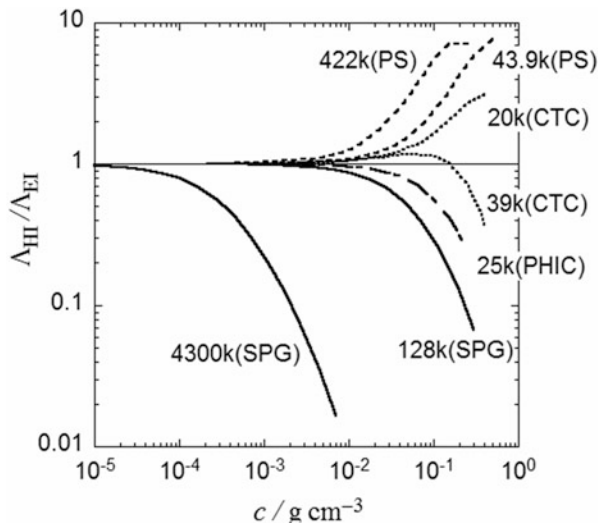
Fig. 2.16 Ratio of the factor Λ_{HI} originated from the hydrodynamic interaction to the factor Λ_{EI} from the entanglement interaction for SPG (*solid curves*), PHIC (*dot-dash curve*), CTC (*dotted curves*), and PS (*dashed curves*) in solution. Λ_{HI} for PS and CTC at 20 k were calculated by Eq. 2.49 including c^2 term

2.8 Conclusions

Naturally occurring polysaccharides have a variety of the chain conformation. Schizophyllan (or scleroglucan with the same chemical structure but different origin), xanthan (xanthan gum), and succinoglycan are rigid helical polymers with large persistence length q, On the other hand, amylose and pullulan are flexible polymers, of which persistence length is as small as that of PS. Cellulose and its derivatives (including CTC), as well as hyaluronic acid, are known as semiflexible polymers with intermediate q values.

The present chapter introduced molecular theories to formulate the intrinsic viscosity $[\eta]$, the Huggins coefficient k', and the zero-shear viscosity η at finite concentrations. According to the theories, $[\eta]$ for the rigid helical polymers are more strongly dependent on the molecular weight than those of more flexible polysaccharides. Therefore, the stiffer polysaccharides with high molecular weights are more suitable as the viscosity enhancement reagent.

Polysaccharide solution viscosities exhibit strong molecular weight and polymer concentration dependences. The molecular theory explained in the present chapter teaches us that those strong dependences arise from both entanglement and hydrodynamic interactions among polymer chains in the solution. The contribution of the entanglement interaction to the solution viscosity is more important than the contribution of the hydrodynamic interaction for stiff polymer solutions, but opposite for flexible polymer solutions. We can anticipate the effectiveness of

newly found polysaccharides as the viscosity enhancement reagent, if we know the molecular characteristics of the polysaccharides.

References

1. Brant D. A., ed, "*Solution Properties of Polysaccharides*," ACS Symp. Ser., No. 150, Am. Chem. Soc., Washington, D.C., 1981.
2. Yamakawa, H., "*Helical Wormlike Chains in Polymer Solutions*," Springer, Berlin & Heidelberg, 1997.
3. Sato T., Teramoto, A., *Adv. Polym. Sci.*, 1996, 126: 85.
4. Ree, D. A., "*Polysaccharide Shapes*," Outline Studies in Biology, Chapman & Hall, London, 1977.
5. Cohen, M. H., Turnbull, D., *J. Chem. Phys.*, 1959, 31: 1164.
6. De Gennes, P.-G., "*Scaling Concepts in Polymer Physics*," Cornell University Press, Ithaca, 1979.
7. Doi, M., Edwards, S. F., "*The Theory of Polymer Dynamics*," Oxford University Press, Oxford, 1986.
8. Yamakawa, H. "*Modern Theory of Polymer Solutions*," Harper & Row Publishers, New York, 1971.
9. Sato, T., *Kobunshi Ronbunshu*, 2012, 69: 613, and the references therein.
10. Beenakker, C. W. J., *Physica A*, 1984, 128: 48.